


Article

Evolutionary Conservation of Photophore Ultrastructure in Sharks: The Case of a Dalatiid Squalomorph

Laurent Duchatelet ^{1,*}, Charlotte Nuyt ^{1,†}, Nathan Puozzo ², Jérôme Mallefet ¹ and Jérôme Delroisse ^{2,*}

¹ Marine Biology Laboratory, Earth and Life Institute, Université catholique de Louvain—UCLouvain, 1348 Louvain-La-Neuve, Belgium

² Biology of Marine Organisms and Biomimetics, Research Institute for Biosciences, University of Mons—UMONS, 7000 Mons, Belgium

* Correspondence: laurent.duchatelet@uclouvain.be (L.D.); jerome.delroisse@umons.ac.be (J.D.)

† These authors contributed equally to the work.

Abstract: Bioluminescence is a common ecological trait among many marine organisms, including three shark families: Etmopteridae, Dalatiidae, and Somniosidae. The kitefin shark, *Dalatias licha* (Bonnaterre, 1788), from the Dalatiidae family is the largest known luminous vertebrate. This study compares the light organ ultrastructure of *D. licha* with that of *Etmopterus spinax*, the type species of Etmopteridae, to gain a deeper understanding of the light emission process and its evolutionary conservation within shark families. The ultrastructure of *D. licha*'s photophores and the morphological changes that occur after hormonal stimulation (via melatonin and α -MSH, which stimulate or inhibit the bioluminescence, respectively) were examined. The photophores consist of a spherical pigmented sheath surrounding a unique, regionalized light-emitting cell (photocyte). The photocyte's basal area contains a specific area filled with granular inclusions that resemble the glowon-type microsomes of *E. spinax*, suggesting that this area is the intracellular site of light emission. An acidophilic secretion, not present in Etmopteridae, is also observed within the granular area and may be involved in photogenesis. The ultrastructure analysis reveals no lens cells or reticular layer, unlike in Etmopteridae photophores, indicating a simpler organization in Dalatiidae photophores. Melatonin stimulation causes the removal of pigments from the photophore-associated melanophores and an increase in the granular inclusion diameter and coverage in the granular area, further showing that this last area is the potential site of light emission, while α -MSH stimulation causes the extension of the melanophore pigments and a decrease in the granular inclusion diameter and coverage. These results support the evolutive conservation of photophore functional organization across luminous etmopterid and dalatiid sharks.

Keywords: bioluminescence; elasmobranch; electron microscopy; photophore; photocyte; dalatiidae



Citation: Duchatelet, L.; Nuyt, C.; Puozzo, N.; Mallefet, J.; Delroisse, J. Evolutionary Conservation of Photophore Ultrastructure in Sharks: The Case of a Dalatiid Squalomorph. *Fishes* **2023**, *8*, 87. <https://doi.org/10.3390/fishes8020087>

Academic Editor: Abbott

Peter Klimley

Received: 23 December 2022

Revised: 29 January 2023

Accepted: 30 January 2023

Published: 1 February 2023



Copyright: © 2023 by the authors. Licensee MDPI, Basel, Switzerland. This article is an open access article distributed under the terms and conditions of the Creative Commons Attribution (CC BY) license (<https://creativecommons.org/licenses/by/4.0/>).

1. Introduction

The ability to emit visible light is a common feature in many phylogenetically distinct deep-sea species [1,2]. Bioluminescent taxa possess a wide range of light emission mechanisms, clearly illustrating the ecological importance of this ability [3–5]. Structures involved in luminescence are diverse, from single cells called photocytes as observed in ctenophores and anthozoans, to complex organs generically called photophores in crustaceans, cephalopods, bony fishes, and elasmobranchs [1,6–11]. Complex photophores are often composed of numerous photocytes, the photogenic cells encased in the organ core surrounded by different structures that enhance the light emission efficiency, such as reticular reflecting and pigmented layers, lenses, or wavelength-selective filters. In some species (mainly bony fish and cephalopods), light emission is mediated via symbiotic luminescent bacteria, and bacterial photophores are specifically dedicated to this symbiosis [6,12–14]. Other organisms can produce their own bioluminescent light within photocytes (i.e., autogenic photophores) [15–20]. Photophore location, number, and size greatly differ between

different species. For example, most of the deep-sea oplophorid shrimps display autogenic photophores spread across the entire shrimp body and appendages, from single isolated photophores with a unique photocyte to photophore clusters [15,16]. In bioluminescent bony fishes, autogenic photophores also present in diverse locations and are complex, presenting diverse structures such as reflectors or lenses [17–20]. The characterization of the ultrastructure and dynamic changes during the luminescence of a photophore allows a deeper morpho-functional understanding of the luminescence process.

Within deep-sea luminous taxa, luminous sharks are encountered in three Squaliformes families: the Etmopteridae, the Dalatiidae, and the Somniosidae (Somniosidae are, however, paraphyletic) [21]. Up to now, all etmopterid and dalatiid species were assumed to be luminous, while only one somniosid species, *Zameus squamulosus*, was described as bioluminescent [21,22]. Shark luminescence is hormonally controlled. Melatonin (MT) triggers a long-lasting glow, while adrenocorticotrophic hormone (ACTH) and alpha-melanocyte-stimulating hormone (α -MSH) inhibit it [21,23,24]. Prolactin was also demonstrated to activate the light production in etmopterids, while it decreases bioluminescence in a dalatiid species, *Squaliolus aliae* [25]. The main bioluminescence function in sharks is counterillumination. The sharks are emitting light that mimics the environmental surrounding light to camouflage themselves from predators or approach benthic preys [21,26]. This function is assumed by minute photophores spread mainly within the ventral integument [21]. Although the function is assumed to be conserved, histological differences in the photophore structure exist between luminous shark families [21]. One of the first descriptions of etmopterid photophores revealed a cup-shaped organ composed of multiple photocytes surrounded by a pigmented layer, surmounted by an iris-like structure (ILS), and topped by lens cells [27]. The ontogenic development of the velvet belly lanternshark, *Etmopterus spinax*, photophores supports this description with (i) the formation of a pigmented layer, (ii) followed by the emergence of protophotocytes and lens cells, (iii) then the maturation of photocytes which start to produce light when green-fluorescent vesicles appear [28]. More recently, the Etmopteridae photophore ultrastructural organization and cytological changes occurring during light emission were investigated in *E. spinax* [11,29]. A thin reflective guanine layer upholstering the pigmented layer was highlighted and assumed to redirect the emitted light to the outside of photophores [11]. Moreover, the intracellular organization of the photocyte was described and appears to be regionalized with a basal area occupied by an ovoid nucleus, a highly vesiculated medial area (vesicular area), and an apical area displaying numerous small granular inclusions (granular area) [11]. This last area was assumed to be the intracellular site of the luminescence reaction in lanternsharks and the granular microsource inclusions of photogenesis were named *glowons* [11]. The analysis of photocyte cytological changes demonstrated a modification of the inclusion density during hormone-induced luminescence [29]. Changes also occur within the ILS area during light emission. This pigmented cellular area plays a role in the propagation of light by acting as a shutter diaphragm to regulate the amount of light reaching the outside [24,29,30]. Ultrastructurally depicted as displaying two different types of melanocyte-like cells, the ILS has been shown to open when the photophore is producing light, resulting in a luminescence intensity increase via motions of pigmented granules along the pseudopodial projections of the melanocyte-like cells [29,30].

Conversely to the etmopterid shark, only standard histology is depicted for dalatiid and somniosid photophores. The first descriptions of dalatiid photophores date back to the 18th century for *Squaliolus* and *Euprotomicrus bispinatus* [31,32]. Interestingly, the single photocyte is composed of a nucleus, a cytoplasmic area, and a large acidophilic secretion in *E. bispinatus* [30]. The general morphology of photophore was also investigated in a few other species (i.e., *Isistius brasiliensis* and *Dalatias licha*): a round-shaped organ composed of a single photocyte embedded in a pigmented sheath and surmounted by lens cells [26,33]. The photophore morphogenesis during the embryogenesis of *Squaliolus aliae* follows the same four steps as the development of photophores in *Etmopterus spinax* [34]. The morphology of the *Zameus* photophore is similar to that of the light organ of dalatiids [22]. Both

families have significantly smaller photophores (i.e., 40 to 83 μm mean diameter depending on the species) than the etmopterid (i.e., 150 μm mean diameter) [21]. As an exception, two dalatiid genera, *Euprotomicroides* and *Mollisquama*, present abdominal and pectoral glands, respectively, which excrete a luminous fluid in addition to putative classical ventral photophores [35].

The present work aims to ultrastructurally depict the photophore of the dalatiid *D. licha* to describe the different components with an emphasis on the intracellular organization of the single photocyte. Cytological changes after hormonal treatments triggering or inhibiting luminescence production are highlighted, and a comparative aspect with the previously described etmopterid photophore is also presented. These results improve our knowledge and understanding of the bioluminescence process occurring in these integumental photogenic structures and give valuable insights into the evolution of light organs in luminescent sharks.

2. Materials and Methods

2.1. Specimen Sampling

A total of 37 specimens of *Dalatias licha* were captured as by-catch off the coast of eastern New Zealand during the Chatham Rise Trawl campaign on board the R.V. Tangaroa in January 2020 [26]. Kitefin shark capture occurred at depths ranging from 443 to 997 m. Sharks were euthanized following a full incision of the spinal cord at the level of the first vertebrae, according to the European regulation for animal research handling. For this study, fresh ventral skin patches bearing photogenic structures of three specimens were dissected using a metal cap driller (6 mm diameter), rinsed in shark saline [292 mmol L⁻¹ NaCl, 3.2 mmol L⁻¹ KCl, 5 mmol L⁻¹ CaCl₂, 0.6 mmol L⁻¹ MgSO₄, 1.6 mmol L⁻¹ Na₂SO₄, 300 mmol L⁻¹ urea, 150 mmol L⁻¹ trimethylamine *N*-oxide, 10 mmol L⁻¹ glucose, 6 mmol L⁻¹ NaHCO₃; total osmolarity, 1.080 mOsmol; pH 7.7 [36]], and then either directly fixed (control) or subjected to hormonal treatments. To trigger light emission, skin patches were immersed in 200 μL of a solution of MT 10⁻⁶ mol L⁻¹ (M5250, Merck, Darmstadt, Germany) for 5 min, and then fixation occurred. To analyze the effect of luminescence inhibition by α -MSH, skin patches were first bathed in 100 μL of MT solution (10⁻⁶ mol L⁻¹) for 5 min, after which 100 μL of an α -MSH 10⁻⁶ mol L⁻¹ (M4135, Merck, Darmstadt, Germany) solution was added, then skin patches were fixed. For all skin patches, fixation was made in a solution of glutaraldehyde (3% glutaraldehyde, sodium cacodylate 100 mmol L⁻¹, NaCl 0.27 mol L⁻¹; pH 7.8) for at least three hours. Skin patches were rinsed in a cacodylate buffer (sodium cacodylate 200 mmol L⁻¹, NaCl 310 mmol L⁻¹; pH 7.8) and stored in the same buffer until used.

2.2. Microscopy Observation

Samples were bathed in a decalcifying solution (OsteoRAL Fast decalcifier for Large Anatomical Specimens; RAL diagnostics, Martillac, France) with stirring in a cold room with solution changes every 2 days for 10 days to ease sectioning. Then, samples were post-fixed in osmium tetroxide (1% osmium tetroxide, sodium cacodylate 100 mmol L⁻¹, Sodium chloride 270 mmol L⁻¹; pH 7.8) for 45 min, followed by progressive dehydration in graded ethanol series. Skin patches were then embedded in a Spurr's resin (EM0300, Merck, Darmstadt, Germany) following [11]. Semithin sections of 600 nm were obtained using a Leica Ultracut UCT ultramicrotome (Leica Microsystems, Wetzlar, Germany) and mounted in glass slides (VWR[®] Microscope slides, VWR, Rosny-sous-bois, France). Then, sections were colored with a 1/1 mixture of 1% methylene blue and 1% toluidine blue in distilled water and observed under a stereomicroscope (Zeiss Axio Scope A1, Zeiss, Oberkochen, Germany) coupled with an AxioCam 305 color camera (Zeiss). Ultrathin sections of 100 nm were also obtained using a Leica Ultracut UCT ultramicrotome (Leica) and delicately placed on copper grids. Sections were subjected to uranyl acetate contrast solution [uranyl acetate solution 180 mmol L⁻¹ in ethanol (2:1)] for 1 h, followed by a bath in lead citrate (lead citrate 80 mmol L⁻¹, sodium citrate 120 mmol L⁻¹, NaOH 160 mmol L⁻¹)

for a duration of 4 min, and left to dry. Sections were observed in a transmission electron microscope (Zeiss Leo 906E, Zeiss, Oberkochen, Germany) coupled with a Jenoptik camera (Jenoptik ProgRes[®] CFcool, Iéna, Germany) and micrographied. Finally, a 3D model of the photophore structural components was performed using the Blender software (Blender Foundation, Amsterdam, The Netherlands, version 2.68).

2.3. Micrography Analyses

Semithin sections were used to measure the mean diameter of the photophore and the different associated structures (photocyte, pigmented zone). Micrographs of ultrathin sections allowed us to measure the diameter (μm), coverage (%), density (count per μm^2), and surface (μm^2) of granular inclusions under the three treatments (i.e., control, melatonin, and α -MSH). Measurements were obtained via micrography analyses on ImageJ software [37]. A total of 44 and 18 different photophores (obtained from 3 individuals) were analyzed for semithin and ultrathin sections, respectively.

Comparisons between the different measurements for each treatment were performed on Rstudio [38] using Student's *t*-tests. Statistical parameters were obtained through Bartlett's and Levene's tests. Statistical difference was considered significant when the *p*-value was under 0.05.

3. Results

3.1. Photophore Ultrastructure

Histological results allow us to observe spherical-shaped photophores of *D. licha* located within the stratified squamous epidermis near the basement membrane (Figure 1B,C). Serialized sections across the skin allow the 3D reconstruction of the light organ. Photophores (diameter of $60.86 \pm 1.26 \mu\text{m}$, $N = 44$ observed photophores, Supplementary File S1) are composed of a unique photogenic cell encased in a spherical layer of pigmented cells. No other components, such as a reticulated reflecting layer or lens cells, are observed. The photocyte diameter is, on average, $36.45 \pm 1.05 \mu\text{m}$ ($N = 44$ observed photocytes, Supplementary File S1), and this unique luminous cell is regionalized and displays different structural components: a basal granular area filled with granular inclusions that are irregularly shaped, dense to electrons, and spread in a white appearing lumen (no electron absorbance), and an apical vesicular area including the ovoid nucleus and a dense mesh of vesicles (Figure 1D). In the granular area of untreated photophore, the following values were measured: mean coverage of $11 \pm 3\%$, granular inclusion density of $2.79 \pm 0.63 / \mu\text{m}^2$, surface of $0.03 \pm 0.007 \mu\text{m}^2$ ($N = 6$ observed photophores). No membrane separates this area from the remaining cell component though it forms a distinct cytoplasmic area. Within the granular area lays a large round-shaped secretion, highly dense to electrons and colored via the methylene/toluidine staining on ultrathin and semithin sections (Figure 1C,D). The vesicular area contains numerous vesicles of varying shapes as well as grey particles (observed by TEM). The rest of the cytoplasm is continuous with the vesicular zone and completely encircles the granular zone up to the base of the photocyte (Figure 1C–G). The vesicular zone thus delimits the end of the photocyte, and the photocyte membrane can be observed (Figure 1H). Finally, the ovoid nucleus is included within the vesicular zone. The surrounding layer of the photophore is composed of multiple melanophore-like cells that are filled with pigment granules that are electron-dense (Figure 1C,D). These granules are similar in structure to melanin granules.

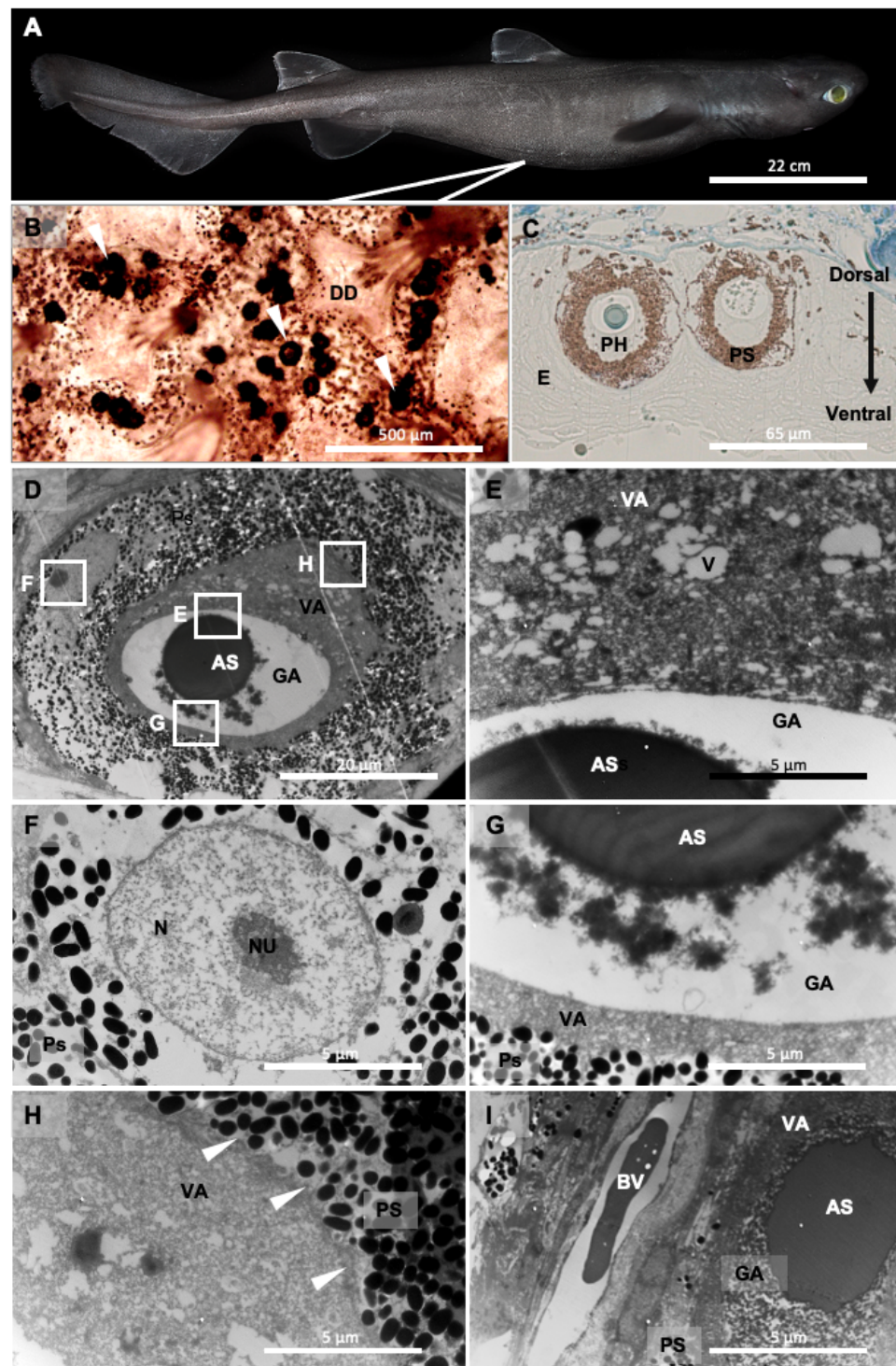


Figure 1. Ultrastructure of *Dalatias licha* photophores. (A) Lateral view of *D. licha*; (B) Upper view of the ventral skin presenting dermal denticles and photophores (arrowhead); (C) Semithin cross-section of *D. licha* photophores; (D) Ultrathin cross-section of *D. licha* photophore with specific highlighted areas (E–I); (E) Close-up on the vesicular area; (F) Close-up on the nucleus of melanophore-like cells constituting the pigmented sheath; (G) Close-up on the granular area; (H) Close-up on the cellular membrane (arrowhead) delimiting the photocyte; (I) Close-up on a blood vessel just aside the photophore. AS, acidic secretion; BV, blood vessel; DD, dermal denticle; E, epidermis; GA, granular area; N, nucleus; Nu, nucleolus; PH, photocyte; PS, pigmented sheath; V, vesicle; VA, vesicular area.

Blood capillaries can be observed under the base of the photophore (Figure 1I). In parallel, the autofluorescence of the photocyte was observed (excitation wavelength: 495 nm, Supplementary Figure S1) mainly around (i.e., within the granular region) and within the acidophilic secretion. Due to the limited number of individuals used in this study, the potential relationship between photophore size and individual size was not investigated.

3.2. Cytological Changes upon Hormonal Treatments

Hormonal treatment with both melatonin (MT) or α -melanocyte-stimulating hormone (α -MSH) showed cytological structural modification within photophores at the level of the pigmented layer, as well as in the granular and vesicular areas. Melatonin-treated photophores present an open-pigmented layer at the photophore apical region (Figure 2). This photophore opening results from the retraction of pigmented granules. These melanophore-like cells act, therefore, as an iris-like structure (ILS). Melatonin-treated tissues present a denser granular area with an increased number of granular inclusions than that observed in control tissues without hormonal treatments. Finally, the vesicular area appears denser to electrons than for control photophores (Figure 2). Treatment with α -MSH results in the dispersion of the ILS-pigmented granules across the melanophore-like projections, with the pigment layer returning to its initial closed spherical shape found in control photophores (Figure 2). At the level of the granular zone, α -MSH-treated tissues show granular inclusions that are more aggregated with each other than control tissues but less dense than what is observed for melatonin-treated tissues. At the level of the vesicular zone, it appears denser than the control photophores but seems to be less dense than what is observed for the melatonin-stimulated photophores. The morphology of the photophore under the inhibitory effect of α -MSH appears to be in a transitional state between a melatonin-stimulated photophore and a control photophore, gradually returning to its initial state without luminescence production. Differences are observed at the level of the vesicles: some photophores under α -MSH treatment show vesicles containing material that could correspond to granular inclusions while other photophores show empty vesicles (Figure 2).

The mean coverage, density of granular inclusions per μm^2 , and surface area of granular inclusions within the granular area were measured for both hormone treatments applied (MT and α -MSH; Figure 3; Supplementary File S2). Under MT treatment, the granular inclusions show significantly higher granular area coverage than after an α -MSH treatment. Even if the density of granular inclusions with MT treatment presents a lower mean value than for α -MSH treatment, this difference is not significant. Finally, the average surface area of the inclusions under MT is significantly larger, which is consistent with a lower density, as the inclusions potentially aggregate with each other.

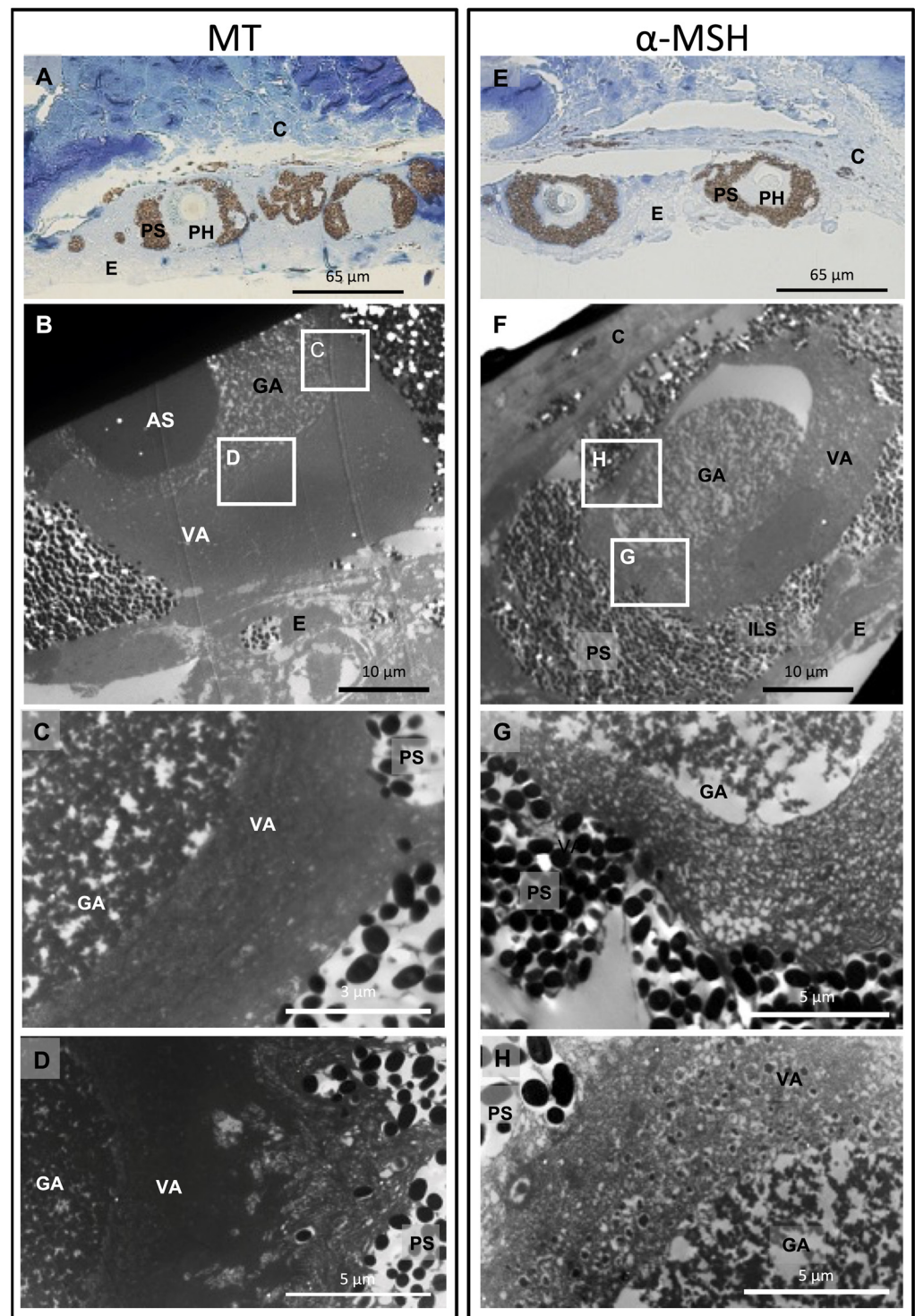


Figure 2. *Dalatias licha* photophore cytological changes occurring during melatonin (MT) and α -melanocyte stimulating hormone treatments (α -MSH). (A) Semithin section across melatonin-stimulated photophores; (B) Ultrathin section across melatonin-stimulated photophore with specific highlighted areas; (C,D) Close-up view of the granular and vesicular areas under melatonin treatment; (E) Semithin section across α -MSH-treated photophores; (F) Ultrathin section across α -MSH-treated photophore with specific highlighted areas; (G,H) Close-up view of the granular and vesicular areas under α -MSH treatment. AS, acidic secretion; C, connective tissue; E, epidermis; GA, granular area; ILS, iris-like structure; PH, photocyte; PS, pigmented sheath; VA, vesicular area.

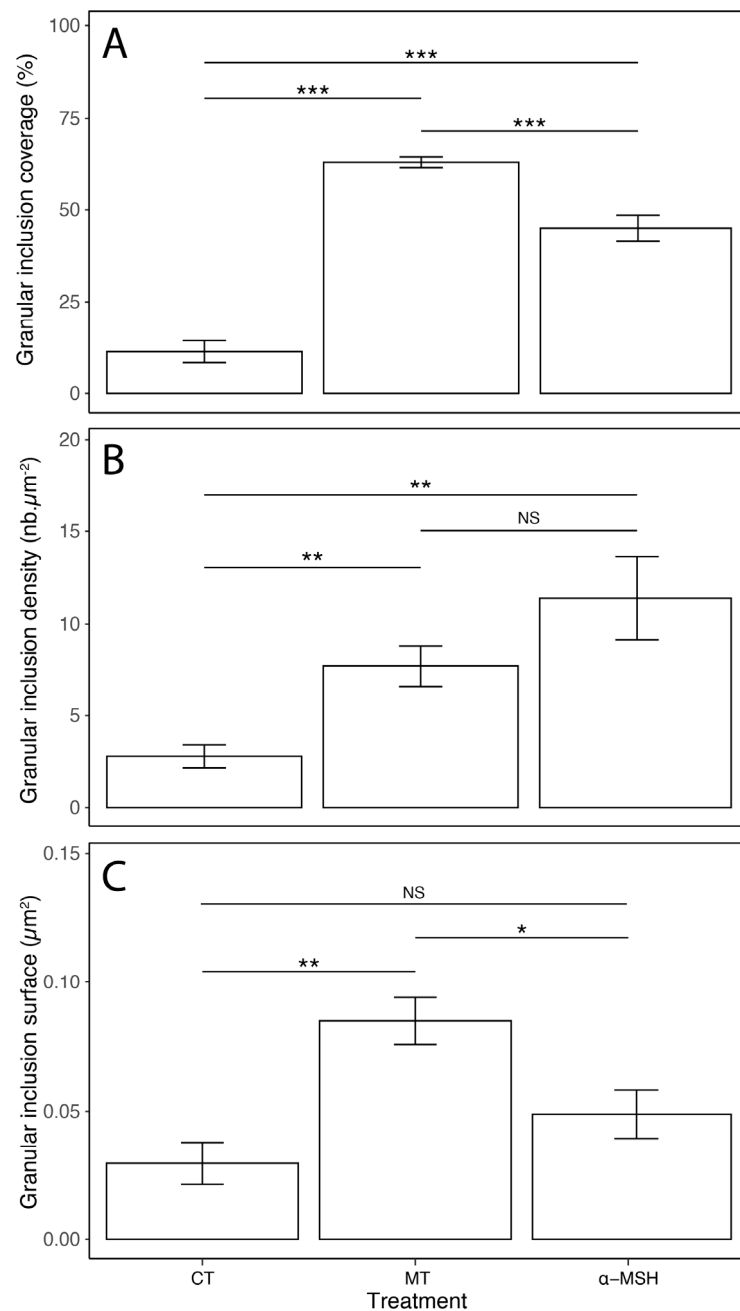


Figure 3. Morphometric data of granular inclusions within the granular area according to hormonal treatments. Measured granular inclusion parameters are (A) the coverage, (B) the density, and (C) the surface. Legend: nb—number of granular inclusions. Error bars represent the standard error (SE); * $p \leq 0.05$, ** $p \leq 0.01$, *** $p \leq 0.001$, NS not significant.

4. Discussion

Variations in structural components of photogenic cells or organs have already been observed for several organisms under different stimuli. The nervously controlled photophores of the midshipman fish, *Porichthys*, show variation of the photocyte cytoplasmic vesicle numbers upon noradrenergic stimulation [39]. The ophiuroidea, *Amphipholis squamata*, presents successive variations within photocytes during cholinergic stimulation, highlighting the presence of six different types of membrane-bound vesicles. One of these vesicle types was assumed to be the site of light production (i.e., microsource) for this species [40]. Recently, photophores of the counterilluminating deep-sea shrimp, *Janicella spinicauda*, were demonstrated to be light sensitive and that cytological changes occurred during light

emission/perception. The shrimp photophores present an increase in the number and size of Golgi bodies in response to light [16]. All these studies, through ultrastructural analyses, allow us to better comprehend cytological and physiological processes involved during bioluminescence events.

Photophore morphology differs among the three known shark families able to produce light. Classical histology has revealed that Somniosidae and Dalatiidae photophores are composed of a unique photocyte, surrounded by a pigmented sheath, and surmounted by lens cells [21,31]. The Etmopterid photophores display more complex photophores with multiple photocytes (6 to 13) enclosed in a cup-shaped multi-cellular pigmented sheath, surmounted by an ILS and one or several lens cells [21]. The ultrastructure description of *Etmopterus spinax* photophores allowed the discovery of an undescribed structure, the reticular layer, located between the photocytes and the pigmented sheath, probably composed of guanine crystals and hence acting as a reflector [11] (Figure 4). The photocyte intracellular organization appears regionalized in three areas: (i) an apical granular area, (ii) a medial vesicular area, and (iii) a basal area containing the nucleus. The granular area is filled with small granular inclusions which are assumed to be the microsomes, i.e., the sites containing the chemical compounds required for photogenesis [29,41,42]. These granular inclusions have been named glowons, regarding the long-lasting glow displayed by shark photophores. Cytological changes during light emission have been analyzed in these structures, becoming denser and more aggregated. The ILS also shows cytological changes during light emission, the pigmented granules being retracted causing the ILS to open and allow the increase in the luminescence intensity [29].

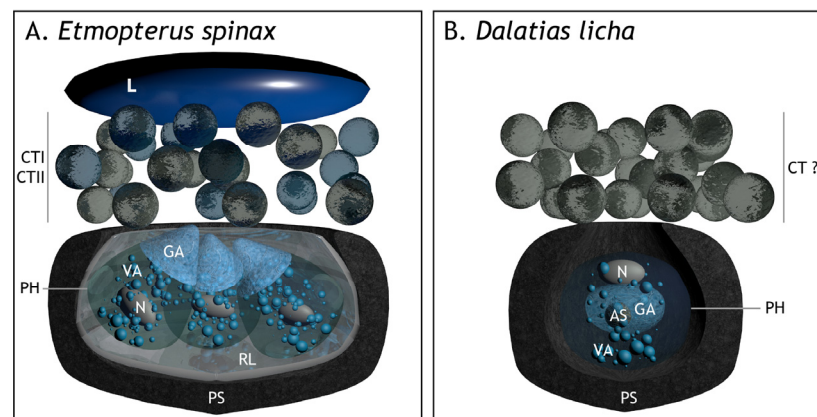


Figure 4. Three-dimensional modelling of the cross-section in (A) *Etmopterus spinax* and (B) *Dalatias licha* photophores based on ultrathin and semithin cross-sections. AS, acidic secretion; CT, cellular type; CTI, CT type I; CTII, CT type II; CT?, putative CT type cells; GA, granular area; ILS, iris-like structure cells; L, lens; PH, photocyte; PS, pigmented sheath; RL, reflective layer; VA, vesicular area.

The present TEM analysis of *D. licha* photophore morphology shows they are composed of an iris-like structure (ILS) associated with a spherical pigmented sheath encompassing one unique regionalized photocyte (Figure 4). The basal zone of the photocyte contains a granular area filled with a large acidophilic secretion and granular inclusions. The latter appears to be similar to the glowon-type microsomes identified in *E. spinax*, and thus these granular inclusions would be the intracellular site of the biochemical bioluminescence reaction [11]. The dense-to-electrons acidophilic secretion located within the bioluminescence reaction site and surrounded by glowons could play a role in photogenesis. This secretion could correspond to the acidophilic secretion described for the *Euprotomicrus bispinatus* (Dalatiidae) photophore [30]. The apical zone contains a centrally positioned nucleus at the apex and numerous vesicles of varying shapes, giving it the name of the vesicular area. The vesicular and granular areas appear distinct but do not appear delimited by a membrane. Contrary to previous studies on the Dalatiidae and Etmopteridae [11,21,26,31–34], the ultrastructure analysis reveals no lens cells at the top of

the photophore of *D. licha*. Furthermore, no reticular layer was identified, contrary to the *E. spinax* photophore (Figure 4).

Interestingly, photocyte green autofluorescence is observed with a gradient of fluorescence (i.e., high autofluorescent signal in the basal region of the photocyte) in *E. spinax* [43] and a more central fluorescence in *D. licha*. In *D. licha*, the acidophilic secretion also exhibits a strong autofluorescence, raising questions about the potential physiological role of this cellular structure. It could indeed be hypothesized that the acidophilic secretion constitutes a particular storage site of luminous compounds (i.e., substrates or enzymes). Nevertheless, a completely different role cannot be excluded (e.g., pH cell regulation or hydrophobic molecule storage).

Morphological changes occurring in *D. licha* photophores have been analyzed at the ultrastructural level through melatonin-induced and α -MSH-inhibited luminescence. Pharmacological investigations of *D. licha* bioluminescence control highlight that melatonin produces a long-lasting production of light, while α -MSH drastically inhibits this light production [26]. The ultrastructural analysis showed that these hormonal treatments cause changes within the granular and vesicular areas of the photocyte as well as in the distribution of the ILS-pigmented granules (Figure 2) as depicted for lanternshark photophores. A melatonin-induced luminescence shows an increase in granular inclusion coverage and diameter, thus filling almost entirely the granular area, while α -MSH-inhibited luminescence shows a decrease in these two parameters. *E. spinax* hormone-induced luminescence shows the same type of effect; melatonin induces an increase in the granular inclusion diameter [29]. Within the vesicular area, *D. licha* photophores under melatonin and α -MSH stimulations show cellular activity with, respectively, the presence of empty and filled vesicles, which could illustrate the potential transport of components necessary for photogenesis as it is supposed for *E. spinax* [29] or other species like the cephalopod *Histiotheuthis bonnellii* [44]. During light emission, the *D. licha* ILS shows the same pigmented granules retraction event as *E. spinax* [29], causing the opening of the photophore at the ILS level (Figure 2). During light inhibition, the ILS-pigmented granules disperse back along the ILS pseudopodia-like projections, closing the top of the photophore and regaining a spherical shape. The movement of the ILS is a key mechanism for controlling the intensity of emitted light and had previously been shown in several species of luminous sharks: *S. aliae* [25], *E. splendidus* [45], *E. mollerii* [46], *E. lucifer*, and *E. granulosus* [26].

5. Conclusions

This study improves our understanding of the light-emission process of the deep-sea dalatiids thanks to an ultrastructural description of the *D. licha* photophore. We also investigated the ultrastructural changes occurring within the photophore and its associated structures during hormone-induced light emission.

By comparing the ultrastructure of *D. licha* and *E. spinax*, we found that the photophore of Dalatiidae exhibits structurally simpler photophores than those of the Etmopteridae family, but still comprises common features and similar cellular targets during hormonal control of luminescence. This suggests that these shark families share a common ancestor with luminescent sharks, and that bioluminescence has not evolved independently in these families as previously thought [47,48]. The simpler organization of the Dalatiidae photophore suggests that the common ancestor of luminous sharks certainly had a similar organization.

Our results also support previous findings that granular inclusions within the photophores would constitute the microsources (the so-called “glowons” in *E. spinax*) responsible for light emission in luminous dalatiids. Additionally, our findings underline the evolutionary conservation of the structure responsible for light production in sharks. Further research is needed to uncover the chemical nature of the shark’s luminous system.

Supplementary Materials: The following supporting information can be downloaded at: <https://www.mdpi.com/article/10.3390/fishes8020087/s1>, Supplementary File S1: Morphological measures of (A) photophore diameter (μm), (B) photocyte diameter (μm), and (C) pigmented zone area (μm^2) performed on semi-thin sections of *Dalatias licha* photophores ($N = 44$ observed photophores). Supplementary File S2: Morphological data and statistics performed on the granular inclusions present within the granular area of *Dalatias licha* ultrastructurally-depicted photocytes according to different treatments: control, melatonin (MT), and α -melanocyte stimulating hormone (α -MSH). Data and statistics for (A) the granular inclusion coverage (expressed in %), (B) the granular inclusion density (μm^{-2}), and (C) the granular inclusion surface (μm^2). *** represents statistical differences (ns, non-significant, * $p \leq 0.05$, ** $p \leq 0.01$, *** $p \leq 0.001$). Supplementary Figure S1: Autofluorescence visualization of *Dalatias licha* photophore. Cross-section in a ventral skin photophore (left) and 495 nm excitation wavelength epifluorescence visualization of the same photophore underlying the green autofluorescence around and within the acidophilic vesicle of *D. licha* photocyte (right). Scale bars = 60 μm . AS, acidophilic secretion; C, connective tissue; E, epidermis; ILS, iris-like structure cells; PS, pigmented sheath.

Author Contributions: Conceptualization, L.D., J.M. and J.D.; methodology, L.D. and J.D.; software, L.D., C.N., N.P. and J.D.; validation, L.D. and J.D.; formal analysis, C.N.; investigation, C.N.; resources, L.D., J.M. and J.D.; data curation, C.N.; writing—original draft preparation, L.D., C.N., J.M. and J.D.; writing—review and editing, L.D., C.N., N.P., J.M. and J.D.; visualization, L.D., C.N. and J.D.; supervision, L.D. and J.D.; project administration, L.D. and J.D.; funding acquisition, L.D., J.M. and J.D. All authors have read and agreed to the published version of the manuscript.

Funding: This research was funded by F.R.S.-FNRS, grant number T.0169.20. JM received a travel grant (35401759) from F.R.S.-FNRS Belgium.

Institutional Review Board Statement: Ethical review and approval were waived for this study since all the studied shark specimens were caught as by-catch during the Chatham Rise fish survey.

Informed Consent Statement: Not applicable.

Data Availability Statement: The original contributions presented in the study are included in the article/Supplementary Material, further inquiries can be directed to the corresponding author/s.

Acknowledgments: The authors thank R. O’Driscoll, Program—Fisheries Monitoring NIWA, D. Stevens, researcher at the NIWA, and the scientific staff and crew of the R.V. Tangaroa (TAN2001, Chatham Rise fish survey, NIWA). This study is the contribution BRC #398 of the Biodiversity Research Center (UCLouvain) from the Earth and Life Institute (ELIV) and the “Centre Interuniversitaire de Biologie Marine” (CIBIM).

Conflicts of Interest: The authors declare no conflict of interest.

References

- Haddock, S.H.D.; Moline, M.A.; Case, J.F. Bioluminescence in the sea. *Annu. Rev. Mar. Sci.* **2010**, *2*, 443–493. [[CrossRef](#)]
- Widder, E.A. Bioluminescence in the Ocean: Origins of biological, chemical, and ecological diversity. *Science* **2010**, *328*, 704–708. [[CrossRef](#)] [[PubMed](#)]
- Anctil, M. Physiological control of bioluminescence. *Photochem. Photobiol.* **1979**, *30*, 777–780. [[CrossRef](#)]
- Anctil, M. Neural Control Mechanisms in Bioluminescence. In *Nervous Systems in Invertebrates*; Ali, M.A., Ed.; Springer: Boston, MA, USA, 1987; pp. 573–602.
- Wilson, T.; Hastings, J.W. Bioluminescence. *Annu. Rev. Cell Dev. Biol.* **1998**, *14*, 197–230. [[CrossRef](#)]
- Herring, P.J. Aspects of the bioluminescence of fishes. In *Oceanography and Marine Biology*; Barnes, M., Ed.; Aberdeen University Press: Aberdeen, UK, 1982; pp. 415–470.
- Anctil, M. Ultrastructure of the luminescent system of the ctenophore *Mnemiopsis leidyi*. *Cell Tissue Res.* **1985**, *242*, 333–340. [[CrossRef](#)]
- Germain, G.; Anctil, M. Luminescent activity and ultrastructural characterization of photocytes dissociated from the coelenterate *Renilla köllikeri*. *Tissue Cell* **1988**, *20*, 701–720. [[CrossRef](#)] [[PubMed](#)]
- Hastings, J.W.; Morin, J.G. Bioluminescence. In *Neural and Integrative Animal Physiology*; Prosser, C.L., Ed.; Wiley-Liss: New-York, NY, USA, 1991; pp. 131–170.
- Herring, P.J.; Dilly, P.N.; Cope, C. The photophores of the squid family Cranchiidae (Cephalopoda: Oegopsida). *J. Zool.* **2002**, *258*, 73–90. [[CrossRef](#)]

11. Renwart, M.; Delroisse, J.; Claes, J.M.; Mallefet, J. Ultrastructural organization of lantern shark (*Etmopterus spinax* Linnaeus, 1758) photophores. *Zoomorphology* **2014**, *133*, 405–416. [CrossRef]
12. Haneda, Y.; Tsuji, F.I. Light production in the luminous fishes *Photoblepharon* and *Anomalops* from the Banda Islands. *Science* **1971**, *173*, 143–145. [CrossRef]
13. Tebo, B.M.; Scott Linthicum, D.; Neelson, K.H. Luminous bacteria and light emitting fish: Ultrastructure of the symbiosis. *Biosystems* **1979**, *11*, 269–280. [CrossRef]
14. Haygood, M.G. Light organ symbioses in fishes. *Crit. Rev. Microbiol.* **1993**, *19*, 191–216. [CrossRef] [PubMed]
15. Nowel, M.S.; Shelton, P.M.J.; Herring, P.J. Cuticular photophores of two decapod crustaceans, *Oplophorus spinosus* and *Systellaspis debilis*. *Biol. Bull.* **1998**, *195*, 290–307. [CrossRef] [PubMed]
16. Bracken-Grissom, H.D.; DeLeo, D.M.; Porter, M.L.; Iwanicki, T.; Sickles, J.; Frank, T.M. Light organ photosensitivity in deep-sea shrimp may suggest a novel role in counterillumination. *Sci. Rep.* **2020**, *10*, 4485. [CrossRef]
17. Ancil, M. Development of bioluminescence and photophores in the midshipman fish, *Porichthys notatus*. *J. Morphol.* **1977**, *151*, 363–395. [CrossRef]
18. Cavallero, M.; Mammola, C.L.; Verdiglione, R. Structural and ultrastructural comparison of photophores of two species of deep-sea fishes: *Argyropelecus hemigymnus* and *Maurollicus muelleri*. *J. Fish Biol.* **2004**, *64*, 1552–1567. [CrossRef]
19. Herring, P.J.; Cope, C. Red bioluminescence in fishes: On the suborbital photophores of *Malacosteus*, *Pachystomias* and *Aristostomias*. *Mar. Biol.* **2005**, *148*, 383–394. [CrossRef]
20. Mallefet, J.; Duchatelet, L.; Hermans, C.; Baguet, F. Luminescence control of Stomiidae photophores. *Acta Histochem.* **2019**, *121*, 7–15. [CrossRef]
21. Duchatelet, L.; Claes, J.M.; Delroisse, J.; Flammang, P.; Mallefet, J. Glow on sharks: State of the art on bioluminescence research. *Oceans* **2021**, *2*, 822–842. [CrossRef]
22. Duchatelet, L.; Marion, R.; Mallefet, J. A third luminous shark family: Confirmation of luminescence ability for *Zameus Squamulosus* (Squaliformes; Somniosidae). *Photochem. Photobiol.* **2021**, *97*, 739–744. [CrossRef]
23. Claes, J.M.; Mallefet, J. Hormonal control of luminescence from lantern shark (*Etmopterus spinax*) photophores. *J. Exp. Biol.* **2009**, *212*, 3684–3692. [CrossRef]
24. Duchatelet, L.; Delroisse, J.; Pinte, N.; Sato, K.; Ho, H.-C.; Mallefet, J. Adrenocorticotrophic hormone and cyclic adenosine monophosphate are involved in the control of shark bioluminescence. *Photochem. Photobiol.* **2020**, *96*, 37–45. [CrossRef] [PubMed]
25. Claes, J.M.; Ho, H.-C.; Mallefet, J. Control of luminescence from pygmy shark (*Squaliolus aliae*) photophores. *J. Exp. Biol.* **2012**, *215*, 1691–1699. [CrossRef] [PubMed]
26. Mallefet, J.; Stevens, D.W.; Duchatelet, L. Bioluminescence of the largest luminous vertebrate, the kitefin shark, *Dalatias licha*: First insights and comparative aspects. *Front. Mar. Sci.* **2021**, *8*, 153. [CrossRef]
27. Ohshima, H. Some observations on the luminous organs of fishes. *J. Coll. Sci. Imp. Univ. Tokyo* **1911**, *27*, 1–25.
28. Claes, J.M.; Mallefet, J. Early development of bioluminescence suggests camouflage by counter-illumination in the velvet belly lantern shark *Etmopterus spinax* (Squaloidea: Etmopteridae). *J. Fish Biol.* **2008**, *73*, 1337–1350. [CrossRef]
29. Renwart, M.; Delroisse, J.; Flammang, P.; Claes, J.M.; Mallefet, J. Cytological changes during luminescence production in lanternshark (*Etmopterus spinax* Linnaeus, 1758) photophores. *Zoomorphology* **2015**, *134*, 107–116. [CrossRef]
30. Duchatelet, L.; Sugihara, T.; Delroisse, J.; Koyanagi, M.; Rezsöházy, R.; Terakita, A.; Mallefet, J. From extraocular photoreception to pigment movement regulation: A new control mechanism of the lanternshark luminescence. *Sci. Rep.* **2020**, *10*, 10195. [CrossRef]
31. Hubbs, C.L.; Iwai, T.; Matsubara, K. External and internal characters, horizontal and vertical distributions, luminescence, and food of the dwarf pelagic shark, *Euprotomicrus bispinatus*. *Bull. Scripps Inst. Oceanogr. Univ. Calif.* **1967**, *10*, 1–64.
32. Seigel, J.A. Revision of the dalatiid shark genus *Squaliolus*: Anatomy, systematics, ecology. *Copeia* **1978**, *1978*, 602–614. [CrossRef]
33. Delroisse, J.; Duchatelet, L.; Flammang, P.; Mallefet, J. Photophore distribution and enzymatic diversity within the photogenic integument of the cookie-cutter shark *Isistius brasiliensis* (Chondrichthyes: Dalatiidae). *Front. Mar. Sci.* **2021**, *8*, 627045. [CrossRef]
34. Duchatelet, L.; Ho, H.-C.; Mallefet, J. Photophore morphogenesis and extraocular encephalopsin expression during the embryogenesis of smalleye pygmy shark (*Squaliolus aliae*). *Diversity* **2022**, *14*, 1100. [CrossRef]
35. Claes, J.M.; Delroisse, J.; Grace, M.A.; Doosey, M.H.; Duchatelet, L.; Mallefet, J. Histological evidence for secretory bioluminescence from the pectoral pockets of the American pocket shark (*Mollisquama mississippiensis*). *Sci. Rep.* **2020**, *10*, 18762. [CrossRef] [PubMed]
36. Bernal, D.; Donley, J.M.; Shadwick, R.E.; Syme, D.A. Mammal-like muscles power swimming in a cold-water shark. *Nature* **2005**, *437*, 1349–1352. [CrossRef] [PubMed]
37. Schindelin, J.; Arganda-Carreras, I.; Frise, E.; Kaynig, V.; Longair, M.; Pietzsch, T.; Preibisch, S.; Rueden, C.; Saalfeld, S.; Schmid, B.; et al. Fiji: An open-source platform for biological-image analysis. *Nat. Methods* **2012**, *9*, 676–682. [CrossRef]
38. RStudio Team. *RStudio: Integrated Development for R*; RStudio: Boston, MA, USA, 2020. Available online: <http://www.rstudio.com> (accessed on 23 November 2022).
39. Ancil, M. Ultrastructural correlates of luminescence in *Porichthys* photophores. I. Effects of spinal cord stimulation and exogenous noradrenaline. *Rev. Can. Biol.* **1979**, *38*, 67–80.
40. Deheyn, D.; Mallefet, J.; Jangoux, M. Cytological changes during bioluminescence production in dissociated photocytes from the ophiuroid *Amphipholis squamata* (Echinodermata). *Cell Tissue Res.* **2000**, *299*, 115–128. [CrossRef]

41. Kaskova, Z.M.; Tsarkova, A.S.; Yampolsky, I.V. 1001 Lights: Luciferins, Luciferases, Their Mechanisms of Action and Applications in Chemical Analysis, Biology and Medicine. *Chem. Soc. Rev.* **2016**, *45*, 6048–6077. [[CrossRef](#)]
42. Delroisse, J.; Duchatelet, L.; Flammang, P.; Mallefet, J. Leaving the dark side? Insights into the evolution of luciferases. *Front. Mar. Sci.* **2021**, *8*, 673620. [[CrossRef](#)]
43. Duchatelet, L.; Delroisse, J.; Mallefet, J. Bioluminescence in lanternsharks: Insights from hormone receptor localization. *Gen. Comp. Endocrinol.* **2020**, *294*, 113488. [[CrossRef](#)]
44. Cavallaro, M.; Battaglia, P.; Guerrero, M.C.; Abbate, F.; Levanti, M.B.; Andaloro, F.; Germanà, A.; Laurà, R. New data on morphology and ultrastructure of skin photophores in the deep-sea squid *Histioteuthis bonnellii* (Férussac, 1834), Cephalopoda: Histioteuthidae. *Acta Zool.* **2017**, *98*, 271–277. [[CrossRef](#)]
45. Claes, J.M.; Sato, K.; Mallefet, J. Morphology and control of photogenic structures in a rare dwarf pelagic lantern shark (*Etmopterus splendidus*). *J. Exp. Mar. Biol. Ecol.* **2011**, *406*, 1–5. [[CrossRef](#)]
46. Claes, J.M.; Mallefet, J. Comparative Control of Luminescence in Sharks: New Insights from the Slendertail Lanternshark (*Etmopterus molleri*). *J. Exp. Mar. Biol. Ecol.* **2015**, *467*, 87–94. [[CrossRef](#)]
47. Claes, J.M.; Mallefet, J. Bioluminescence of sharks: First synthesis. In *Bioluminescence in Focus—A Collection of Illuminating Essays*; Meyer-Rochow, V.B., Ed.; Research signpost: Kerala, India, 2009; pp. 51–65.
48. Straube, N.; Iglésias, S.P.; Sellos, D.Y.; Kriwet, J.; Schlieven, U.K. Molecular phylogeny and node time estimation of bioluminescent lantern sharks (Elasmobranchii: Etmopteridae). *Mol. Phylogenet. Evol.* **2010**, *56*, 905–917. [[CrossRef](#)] [[PubMed](#)]

Disclaimer/Publisher’s Note: The statements, opinions and data contained in all publications are solely those of the individual author(s) and contributor(s) and not of MDPI and/or the editor(s). MDPI and/or the editor(s) disclaim responsibility for any injury to people or property resulting from any ideas, methods, instructions or products referred to in the content.